Applied Surface Science 491 (2019) 595–606

Contents lists available at ScienceDirect

Applied Surface Science

journal homepage: www.elsevier.com/locate/apsusc

Full length article

New insight into the mechanism of $LiPO_2F_2$ on the interface of high-voltage cathode $LiNi_{0.5}Mn_{1.5}O_4$ with truncated octahedral structure

Dongni Zhao[a], Sainan Song[c], Xiushen Ye[b], Peng Wang[a], Jie Wang[a], Yuan Wei[a], Chunlei Li[a], Liping Mao[a], Haiming Zhang[b], Shiyou Li[a,*]

[a] College of Petrochemical Technology, Lanzhou University of Technology, Lanzhou 730050, PR China
[b] CAS Key Laboratory of Comprehensive and Highly Efficient Utilization of Salt Lake Resources, Qinghai Institute of Salt Lakes, Chinese Academy of Sciences, Xining 810008, PR China
[c] Lanzhou Petrochemical Research Center, Petrochina, Lanzhou 730060, PR China

ARTICLE INFO

Keywords:
$LiPO_2F_2$
$LiNi_{0.5}Mn_{1.5}O_4$
Electrolyte additive
Common ion effect
Interface film

ABSTRACT

The development of high energy density material is of great importance and urgency for new generation of energy storage system. However, electrolyte formula for high voltage system remains a challenge. The use of various functional additives gives rise to the complexity of electrolyte system and hinders completely understanding of the action mechanism of additives. Herein, we report the adaptability and mechanism of a single additive $LiPO_2F_2$ added in the conventional $LiPF_6$-based electrolyte system. The resulting conclusion displays a notable improvement in the cycling stability for 5 V-class cathode $LiNi_{0.5}Mn_{1.5}O_4$, the capacity retention increase from 85.76% to 95.92%. It is comforting that the rate performance is not reduced due to the increase in cycle stability, and it also shows good advantages in terms of high rate and reversibility. Meanwhile, detailed analysis about interface mechanism for $LiPO_2F_2$ by the surface testing (SEM, TEM and XPS) give the direct characterizations. Common ion effect of the decomposition product Li_3PO_4 from additive is probed from the above characterization and combined with DFT calculations and some clever experiments to prove the positive effect of additives. The findings obtained from this work may provide a useful guidance for the research on electrolyte formulation for high voltage system.

1. Introduction

Lithium-ion batteries have become an important driving force for the development of electric vehicles due to their high energy and power density compared with other energy storage devices. In order to meet the energy and power requirements of electric vehicles, especially in the pursuit of cruising endurance mileage and accelerated climbing performance, a new generation of lithium-ion battery materials is required to have higher power performance. The strategy to improve battery power performance can be summarized as two aspects: one is to improve the operating voltage of the battery, and the other is to improve the battery's ability to withstand high current charge and discharge. The spinel manganese-based positive electrode material is preferred as a positive electrode material for a power type lithium ion battery because of its low cost, safety, low toxicity, and high thermal stability, particularly a three-dimensional tunnel structure that facilitates lithium ion transport. However, the working voltage of spinel $LiMn_2O_4$ is 4.0 V, which the dissolution of Mn^{3+} and Jahn-Teller distortion occur during charging and discharging, and the high temperature performance is poor, which limits its further application [1–2]. The redox process of spinel $LiNi_{0.5}Mn_{1.5}O_4$ occurs only at the Ni site, which reduces the production of Mn^{3+} cations and its associated Jahn-Teller effect. In addition, $LiNi_{0.5}Mn_{1.5}O_4$ has a higher charge and discharge plateau (about 4.7 V), and the actual specific energy density is 658 Wh kg^{-1}, which is higher than those of other commercial cathode materials ($LiMn_2O_4$ is 440 Wh kg^{-1}; $LiFePO_4$ is 500 Wh kg^{-1}). Therefore, $LiNi_{0.5}Mn_{1.5}O_4$ is considered to be the most promising cathode material candidate for power lithium-ion batteries.

However, a huge challenge for the commercial application of $LiNi_{0.5}Mn_{1.5}O_4$ is that the assembled battery at a high voltage of 4.5 V or higher will have a decrease in cycle performance, a decrease in coulombic efficiency, and a decrease in capacity [3]. Studies have shown that charging $LiNi_{0.5}Mn_{1.5}O_4$ battery at high voltage accelerates the oxidation of the electrolyte and results in the formation of a high-impedance cathode electrolyte interface (CEI) film on the electrode surface. The HF acid produced by the oxidative decomposition of the

* Corresponding author at: College of Petrochemical Technology, Lanzhou University of Technology, 36 Pengjiaping Road, Lanzhou, Gansu province, PR China.
E-mail address: lishiyoulw@163.com (S. Li).

https://doi.org/10.1016/j.apsusc.2019.06.146
Received 15 May 2019; Received in revised form 6 June 2019; Accepted 13 June 2019
Available online 18 June 2019
0169-4332/

electrolyte accelerates the deterioration of the material cycle performance at high voltage, and also generates gases to cause bulging and swelling of the battery [4]. Further, the formation of HF acid reacts with $LiNi_{0.5}Mn_{1.5}O_4$ to cause the dissolution of Mn and Ni. The dissolved products (such as LiF, MnF_2, NiF_2, etc.) and the organic polymer formed by the decomposition of the electrolyte will deposit on the surface of $LiNi_{0.5}Mn_{1.5}O_4$, resulting in continuously thickening the CEI film, and the impedance is continuously increased which causes the aggravation of battery performance [5]. From the above failure mechanism, the degradation of the cycle performance of $LiNi_{0.5}Mn_{1.5}O_4$ is mainly related to the side reaction caused by direct contact between the electrode and the electrolyte. Therefore, researchers have proposed various methods to suppress side reactions at the electrode and electrolyte interface, for example, to optimize particle size and coating surface modification [6–10]. However, it is often difficult to expand to large-scale battery applications because the synthesis process is complicated and the discharge capacity of the high-voltage material is sometimes lowered. The development of a high-voltage electrolyte that is compatible with the positive electrode material has become an effective strategy for improving the performance of the $LiNi_{0.5}Mn_{1.5}O_4$ battery due to its high efficiency and convenience. Research on improving the performance of high-voltage battery CEI film can be carried out in two aspects: the substitution of carbonate solvents by dinitrile [11], sulfone [12] or ionic liquid solvents [13] can reduce the decomposition of electrolyte and form a stable CEI film. It is also possible to introduce a novel film-forming additive lithium salt such as lithium difluoro(oxalate)borate (LiODFB) [14], lithium tetrafluorobarbate (LiFOP) [15], lithium 4-pyridine trimethyl borate (LPTB) [16] and lithium catechol dimethylborate (LiCDMB) [17], which can preferentially oxidize on the surface of the positive electrode before oxidative decomposition of the solvent, and the products deposit on the surface of the positive electrode to form a dense protective layer. Thereby it can inhibit the further oxidation of electrolyte components.

The components of the CEI film in the lithium ion battery are mainly: inorganic components such as LiF, Li_2O, $Li_xPO_yF_z$, Li_xPF_y, Li_2CO_3, and organic components such as $ROCO_2Li$, $(CH_2OCO_2Li)_2$, ROLi [18]. Among them, $Li_xPO_yF_z$ is considered to be a very critical component. Andersson et al. [19] reported that the source of the $Li_xPO_yF_z$ component is the hydrolysis of $LiPF_6$. Zhang et al. [20] found that when 1,3-propane sultone and vinylene carbonate (VC) were used as dual-function electrolyte additives, the increase in $Li_xPO_yF_z$ concentration in the CEI layer helped to increase capacity retention and coulomb effectiveness. Similarly, Li et al. [21] found that 1-propylene-1,3 sultone was used as an electrolyte additive, and the CEI film component contained more $Li_xPO_yF_z$, which could improve the cycling stability of $LiCoO_2$/graphite battery at a high voltage of 4.5 V. Therefore, it can be inferred that if $Li_xPO_yF_z$ containing in the SEI layer has relative thermodynamic stability, the side reaction between the electrode and the electrolyte can be effectively suppressed and the cycle performance of the battery can be improved. Kim et al. [22] proved that VC and lithium difluorophosphate ($LiPO_2F_2$) act as a co-reducing agent, which can hinders the charge transfer on the graphite surface and forms a surface film with good ion conductivity on the graphite surface to improve the rate performance of the battery. The experiment operated by GH Yang et al. [23] proved that the capacity retention of graphite/Li half-cell with electrolyte adding 1.6 wt% $LiPO_2F_2$ increased from 82.53% to 98.04% after 160 cycles, while the capacity retention of $LiCoO_2$/Li half-cell increased from 89.60% to 97.53%. Electrochemical impedance spectroscopy and DFT calculations show that the SEI layer containing $LiPO_2F_2$ can reduce the surface impedance of the battery in the final stage of the cycle and maintain the cycle stability of the battery. Yang, Zhao and Liu applied $LiPO_2F_2$ as an electrolyte additive to $LiNi_{0.5}Co_{0.2}Mn_{0.3}O_2$/graphite [24], $LiNi_{0.5}Mn_{0.25}Co_{0.25}O_2$ electrode [25] and $Li[Ni_{1/3}Mn_{1/3}Co_{1/3}]$ O_2/graphite systems [26], respectively. It was found that the high and low temperature performance of the battery can be improved by forming a conductive and stable CEI film on the surface of the electrode.

Although $LiPO_2F_2$ as an electrolyte additive has appeared in domestic and foreign reports, as far as we know, there is no distinct interpretation of its action mechanism. This paper will reveal the mechanism of $LiPO_2F_2$ on the $LiNi_{0.5}Mn_{1.5}O_4$ half-cell from a unique perspective on the basis of high voltage system and by the means of quantum chemistry calculation and ingenious methods. It can provide theoretical guidance for building and constructing a high-voltage electrolyte system. In this paper, the common-ion effect is used as a theoretical support. It is believed that Li_3PO_4 preferentially produced in the decomposition products of $LiPO_2F_2$ can inhibit the further decomposition of lithium salt $LiPF_6$. This paper reveals the mechanism of electrolyte additive under autocatalytic decomposition drawing on the idea of coating of cathode material, and provides new ideas for the design and mechanism of additive.

2. Materials and methods

2.1. Materials preparation

The materials preparation mainly includes cathode materials and electrolyte. Cathode material $LiNi_{0.5}Mn_{1.5}O_4$ with truncated octahedral structure is prepared by our laboratory (specific process has been put into supporting information). And 1 M $LiPF_6$-DMC/EC (1:1, by volume) marked as baseline electrolyte was purchased from Chaoyang Yongheng Chemical Co., Ltd. as reference system. 1 wt% $LiPO_2F_2$ (99.5%, Huizhou Dado New Material Technology Co., Ltd) was added in the baseline electrolyte as experimental system, which marked as 1% $LiPO_2F_2$.

The cathode electrode sheet was coated on the aluminum foil by the mixture of 80 wt% LNMO, 10 wt% carbon black and 10 wt% polyvinylidenefluoride (PVDF) on the single side of substrate. CR2025 coin cells were assembled in the argon atmosphere glove box using above prepared cathode material and electrolytes. The mass loading of active material is 1.75 mg cm^{-2}.

2.2. Electrochemical characterizations

Ionic conductivities for two samples were tested by the conductivity meter (DDSJ-308A, Shanghai, China) at ambient temperature.

All the following tests were performed on a CHI660C Electrochemical Workstation (Shanghai, China) through a three-electrode system, which using the pre-prepared LNMO electrode as the working electrode, and lithium sheets both as the reference electrode and counter electrode, respectively. Linear sweep voltammetry (LSV) for the electrolytes was carried out at the scan rate of 2 mV s^{-1} at the voltage range of OCV-7.0 V. The potentiostatic test was tested after pre-cycle and after cycling with fully charging to 5.0 V. Electrochemical impedance spectroscopy (EIS) tests of cells with two electrolytes were measured at the fully delithiated state of 5.0 V at different cycling number over the frequency range of 0.01 Hz to 10^5 Hz, applied with a sinusoidal AC perturbation of 5.0 mV.

Charge-discharge tests and corresponding electrochemical performance testing were performed on the Land cell tester CT2001A (Wuhan, China) in the voltage of 3.5–5.0 V for LNMO/Li half cells. A fresh electrode was divided into two same sizes and then rinsed in the two above-mentioned electrolytes with still in the 40 °C at vacuum drying oven for 3 days. Next, atomic absorption spectroscopy (AAS, Varian 725-ES, USA) was performed on the two samples to detect the dissolution amount of transition metal ion in electrolytes. Cathode electrode was stripped off from the cells after cycling with different electrolyte samples to further analyze the film morphology. Prior to surface analysis, the cathode materials were rinsed with DMC three times to remove adsorbed substances and then place it in an argon-filled glove box and let it dry naturally. The scanning electron microscope (SEM, JSM-6701F, Hitachi, Japan) and transmission electron

microscopy (TEM, JEM-2100, JOEL, Japan) were used to characterize film properties. And X-ray photoelectron spectroscopy (XPS, Axis Ultra DLD, Kratos Analytical Ltd.) was used to detect surface element to obtain surface film composition information.

2.3. DFT calculation

Quantum chemical calculation is to obtain the energy, vibration, thermodynamics and other information corresponding to the structure by solving the Schrodinger equation. In this paper, the mechanism of electrolyte additive on the surface of cathode material is studied by quantum chemical calculation through Gaussian09 software package [27]. The computing environment used in this study was provided by the Chinese National Grid (CNGrid) of the Chinese Academy of Sciences and the Chinese Academy of Sciences Supercomputing Environment (ScGrid) based on SCE software (http://www.cngrid.org, http://www.Scgrid.cn) [28].

The geometrical optimization of all the molecules in the paper is carried out by density functional theory (DFT), B3LYP/6-31 + G(d,p) basis group in the form of closed shell. In order to better match the experimental data, all calculations were performed in an implicit solvation model with a dielectric constant of 46.21 constructed under the PCM method. Since the studied lithium salts were all ionic molecules, the geometry used in the study was the lowest energy conformation of lithium ions at different sites. The molecular configurations with the lowest energy obtained are all without a null-frequency structure. Among them, the molecular volume calculation is based on the molecular surface model constructed by the Marching Tetrahedra algorithm, and all calculations are performed by the Multiwfn software package [29].

The Gibbs free energy in the paper is calculated by the Gaussian-4 (G4) thermodynamic combination method. The calculation process includes: (1) Geometric optimization at the B3LYP/6-31G (2df, p) level; (2) Performing the harmonic vibration analysis of the equilibrium state at the same level as the previous step, and using 0.9854 as the correction parameter for frequency correction, thereby obtaining the corrected zero point energy (ZPE); (3) Using aug-cc-pVQZ and aug-cc-pV5Z for Hartree-Fock energy extrapolation, $E_{HF/limit}(n,n+1) = (E_{HF/n+1}\text{-}E_{HF/n}\ \exp.(-\alpha))/(1\text{-}\exp(-\alpha))$, where $n = 4$, $\alpha = 1.63$; (4) Single point energy calculation at MP4, 6-31G(d) level, and diffusion basis correction, extra pole basic group correction is performed, and the correlation energy correction and high-level base group correction are performed by the coupling cluster method; (5) Spin-orbit coupling correction for atomic systems ; (6) High-order energy correction, $E_e(G4) = E(combined) + E(HLC)$; (7) Finally, the obtained energy level can be summed with the zero point. $E_0(G4) = E_e(G4) + E(ZPE)$ is the high-precision energy information with the accuracy of CCSD(T,full)/$G3_{LargeXP}$ + HF_{limit} level [30,31].

The binding energy calculation in the paper is performed at the B3LYP/6-311 + G(d,p) level. Due to the overlap of the basic functions of the two structural segments in the calculation process, the binding position base group is increased, resulting in the problem of underestimation of the binding energy. Therefore, we added the based group overlap correction (BSSE correction) to get a more accurate information about binding energy, that is $E_{int} = E(AB) - E(A) - E(B) + E_{BSSE}$.

3. Results and discussion

3.1. Evaluation of basic performance for electrolyte

To determine whether the electrolyte formulation is suitable for the LIBs systems, a series of basic properties, such as conductivity, oxidation tolerance, corrosion protection and leakage current for our electrolytes were investigated. Fig. 1a shows the results of the ionic conductivities for two different electrolytes. Compared with baseline electrolyte, the conductivity for 1% $LiPO_2F_2$ electrolyte is some lower. That decrease is due to the fact that the difference in the structure of two different lithium salt (shown in Fig. 1b). From the structure, we can find that the ionic radius of additive $LiPO_2F_2$ is smaller than that of $LiPF_6$ (the Bohr volumes of the two anions $PO_2F_2^-$ and PF_6^- are marked in Fig. 1c, respectively.), resulting in a larger lattice energy, and a less solubility in organic solvents. Then, DFT calculation for dissolution energy was calculated to discriminate the main reason for the reduced conductivity. The corresponding dissolution energy for two lithium salts after structural optimization is shown in Fig. 1c. From the result, it can be concluded obviously that the $LiPO_2F_2$ has higher dissolution energy (−5.790 eV) than $LiPF_6$ (−6.254 eV). These structure properties will cause difficulty in dissociating in the electrolyte. It can be elucidated that the additive is more difficult to dissociate in an organic solvent, which is also the main reason for its addition to lower the conductivity. But even if the conductivity is reduced, it still does not affect the normal adaptation of the electrolyte system for the high voltage system.

Further, we analyzed the oxidation of the two electrolytes on the LNMO surface by testing the LSV on the LNMO electrode (Fig. 1d). From the LSV testing, it can be ascertained that the current continues to increase as the voltage rising. Unlike the baseline electrolyte, a small peak appears near 3.1 V for the electrolyte containing $LiPO_2F_2$ additive, which is thought to be caused by oxidation of the additive. And a possible mechanism reaction formula is shown in Formula (1). PO_2F is a self-decomposition derived from the additive $LiPO_2F_2$, which will be explained in detail later. The oxidation potentials of the two electrolyte systems are basically coincident in the following potential, which have the same peaks around 4.2 V (corresponding to $Mn^{3+} \rightarrow Mn^{2+}$) and 5.0 V (corresponding to $Ni^{4+} \rightarrow Ni^{2+}$). It can be observed that the two characteristic peaks derived from LNMO appear to shift to the high position, which results from the increased polarization at high current. From the results can be concluded that $LiPO_2F_2$ is more preferentially decomposed, and the decomposed product can be covered on the active site of LNMO surface, hindering further decomposition of the electrolyte.

$$2PO_2F \xrightarrow{-2e^-} 2PO_2^+ + F_2 \quad (1)$$

Next, we would like to evaluate the corrosion of the electrolyte to the electrode based on the result of LSV (Fig. 2). We divided the same electrode into two equal masses and soaked them in two electrolytes with the volume of 2 mL, respectively. The reagent bottle containing the electrolyte was sealed and placed in a vacuum oven at 40 °C for about 3 days. Later, we observed that there was a significant change in the color of the two electrolytes. The color of the electrolyte without additives is obviously in deep yellow. It is due to that at the high temperature, the main salt $LiPF_6$ in the electrolyte will undergo the following autocatalytic reaction (2). When a small amount of water appears in the electrolyte, the following reactions (3)–(4) will further occur. From the reaction formula, we can find that a large amount of strong Lewis acid HF is generated in the $LiPF_6$ electrolyte, which will cause severe corrosion on the surface of the metal oxide electrode.

According to other researchers' research, the additive $LiPO_2F_2$ will also decompose in the presence of trace water. The reaction equation is shown in Eq. (5). It can be confirmed that Li_3PO_4 is produced from the decomposition of the additive. According to common-ion effect, it can be analyzed that Li_3PO_4 can effectively inhibit the decomposition of $LiPF_6$ in electrolyte. The principle is that the addition of a strong electrolyte containing the same ions as the electrolyte anion in the electrolyte solution reduces the solubility of the electrolyte. Some researchers have found that Li_3PO_4 has multiple functions on the surface of nickel-rich materials: it absorbs moisture in the electrolyte to reduce the degree of HF, and even eliminates HF, thereby protecting the electrode active material from electrolyte corrosion [32]. This is consistent with the observation from the Fig. 2a, which the electrolyte with $LiPO_2F_2$ additive turn to deep yellow placing in the high temperature.

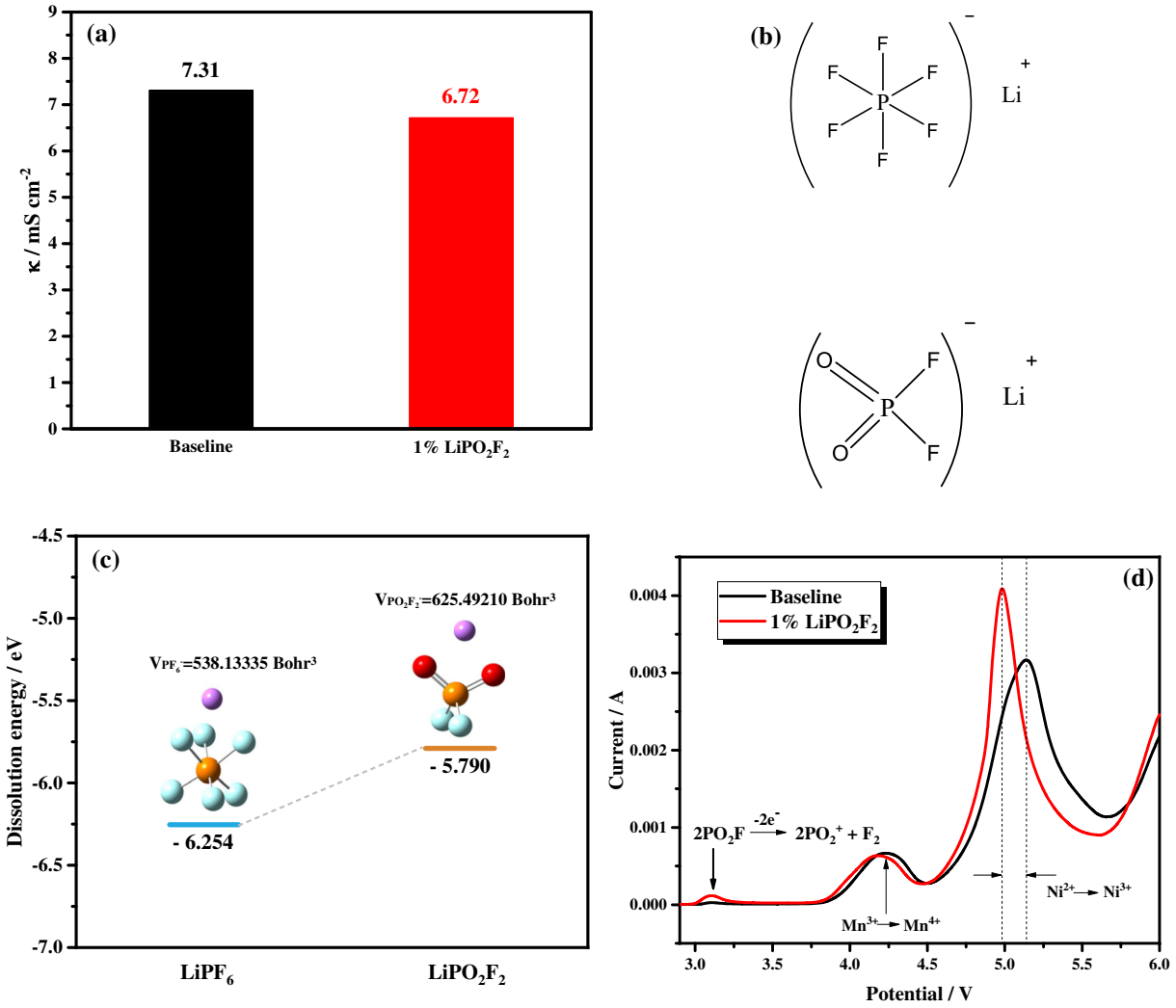

Fig. 1. (a) Ion conductivity at room temperature, (b) molecular structure of two electrolytes; (c) dissolution energy of $LiPO_2F_2$ and $LiPF_6$; and (d) LSV of two electrolytes with the scan rate of 2 mV s^{-1} in the voltage range of OCV-7.0 V performed on LNMO electrode.

To gain more insight, AAS for two electrolytes stood at high temperature were tested to quantitatively analyze the concentration of metal ions in the electrolytes. As a result, it is apparent from Fig. 2b that the transition metal ions of Mn and Ni in the baseline electrolyte are significantly higher than those of the electrolyte system containing the additive. The specific reasons and related mechanisms are also as

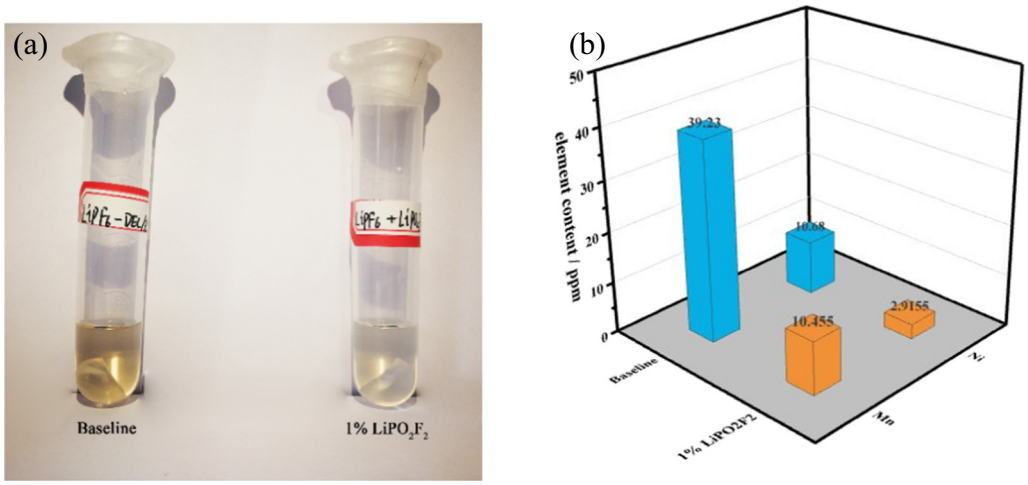

Fig. 2. Corrosion analysis of two electrolytes on the electrode; (a) the color of the electrode sheet is immersed in the electrolyte at 40 °C for 3 days; and (b) the content of transition metal elements of Mn and Ni in the two electrolytes.

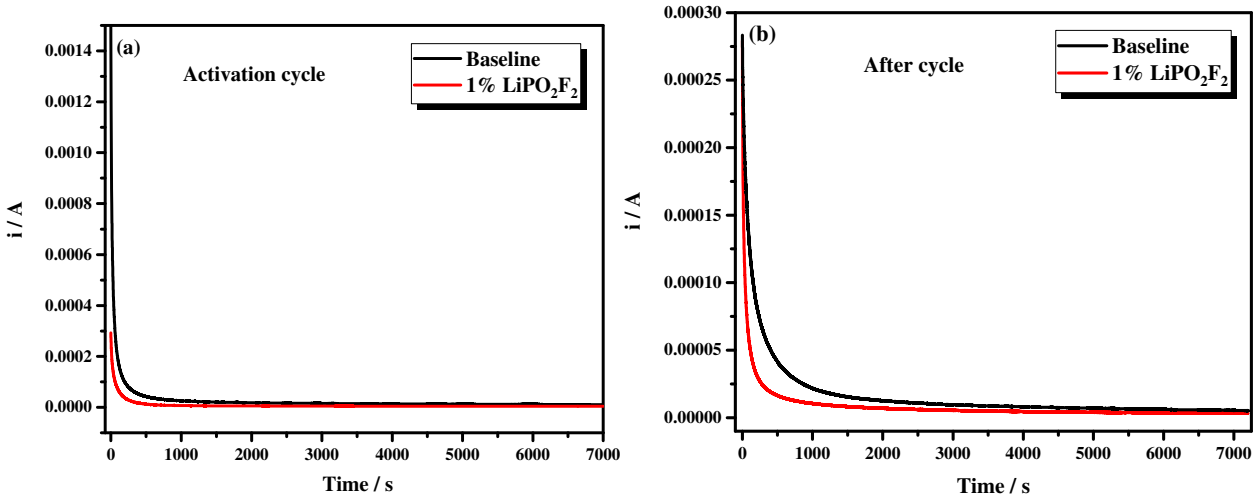

Fig. 3. The leakage current at different condition for two electrolytes (a) pre-cycle; and (b) after cycling.

described above.

$$LiPF_6(sol.) \xrightarrow{\Delta} LiF(s) + PF_5(sol.) \quad (2)$$

$$LiPF_6(sol.) + H_2O \rightarrow POF_3(sol.) + LiF(s) + 2HF(sol.) \quad (3)$$

$$PF_5(sol.) + H_2O \rightarrow POF_3(sol.) + 2HF(sol.) \quad (4)$$

$$2H_2O + PO_2F_2^- + 4Li^+ \overset{e}{\leftrightarrow} Li_3PO_4 + LiF + HF + 3H^+ \quad (5)$$

To achieve a preliminary understanding of film forming property derived from two electrolytes, leakage current was tested at different condition for LNMO/Li half cells. Fig. 3a is the leakage current test of the LNMO/Li half-cell activation cycle of the two electrolytes. Fig. 3a is the leakage current test of the LNMO/Li half-cell of the two electrolytes during activation cycle. It can be analyzed from the results that the leakage currents of the two electrolyte batteries are both low, but the additive electrolyte possess lower leakage current. This indicates that the film come from the additive $LiPO_2F_2$ is better than the baseline electrolyte in suppressing self-discharge of cells, which can reduce the outflow of electrons, and can further reduce the film thickness. Fig. 3b further tests the leakage current of the two electrolytes after the end of the cycle. The positive surface film is considered to have been substantially self-healing. It can be seen that the leakage current is significantly lower than that in the activation cycle, but the film formation of the baseline electrolyte half-cell is much worse than that of the additive electrolyte, and the difference is more pronounced than that in the activation cycle. It can be predicted that the film formed by the additive has a good protective effect on the positive electrode and can suppress the occurrence of self-discharge.

3.2. Electrochemical performance test for LNMO/Li half-cell

After the above evaluation of the basic properties of the two electrolytes, the preliminary prediction of the electrochemical properties of the two electrolytes has been made. This section matches the two electrolytes with the LNMO/Li half-cell and performs a series of evaluations on its electrochemical performance. The deadliest problem with lithium nickel manganese oxide is poor cycle stability, which is due to the incompatibility of electrolyte.

The first charge and discharge curve and efficiency reflect many interface characteristics between electrolytes and electrode materials. Fig. 4a is the first charge and discharge curves for the two electrolytes. From the figure we can see that there is a significant charging plateau at 4.7–4.8 V. The charging plateau of the baseline electrolyte is longer than that of the additive electrolyte, which means that during the first charging process, a large amount of electrolyte in the baseline sample have been decomposed, and the electrolyte with the additive is protected by $LiPO_2F_2$, which causes the decrease in the decomposition. During the process of discharge, the discharge plateau of the additive electrolyte is significantly improved, which indicates that the interface film formed under the action of the additive reduces the loss of irreversible capacity and improves the first efficiency. As can be seen from the data in the figure, the efficiency of the battery after the addition of additive is increased from 56.7% to 71.1%. The discharge process for lithium-ion battery corresponds to the process of lithium ion being embedded from the negative electrode to cathode material, which may have a rearrangement of the material structure, and a good interface film can ensure the structure not being destroyed. Through analysis, we can conclude that the addition of additives optimizes the properties of the interface film during the first film formation process, thereby protecting the structure of the electrode material in the process of structural rearrangement to ensure integrity.

At the same time, we thoroughly analyzed from Fig. 4b the differential capacity curve of the first charge when the two electrolytes were matched with the LNMO/Li half-cell. It can be observed from the figure that the position indicated by the arrow is the reaction potential of the electrolyte and LNMO surface. We mainly analyze the two peaks appearing above 4.6 V, where the peak corresponds to Ni^{2+} to Ni^{3+} and Ni^{3+} to Ni^{4+} in LNMO. We can observe that the peak position of lithium nickel manganese oxide containing additives is relatively high, which indicates that a preferential layer of Li_3PO_4 may be formed on the surface of the electrode after preferential decomposition of the additive, so that the contact between the subsequent electrolyte and the electrode is less. Even if the electrons lost by the solvolysis are also difficult to transport, the potential is high and the potential difference is increased. Through the analysis of the first cycle curve, we can conclude that the addition of additives effectively improves the electrode/electrolyte interface film properties, so that the interface film can protect electrode without affecting the transmission of lithium ions, that is, no affecting the electrochemical properties.

Through the test of the subsequent cycle stability, we obtain the data of the cycle performance in Fig. 4c. The electrolyte system containing additive is beneficial to improve the cycle performance, we can analyze that the capacity of the electrolyte system containing the additive is steadily rising from 40 cycles. This indicates that the interface film derived from the additive is in a process of continuous self-repair. After the modification of the additive, the capacity retention rate of the LNMO/Li half-cell is increased from 85.76% to 95.92%. From the perspective of cycle efficiency, the cycle efficiency of the two electrolytes is relatively stable, and the system containing the additive electrolyte is relatively higher. It can be predicted that the cycle life

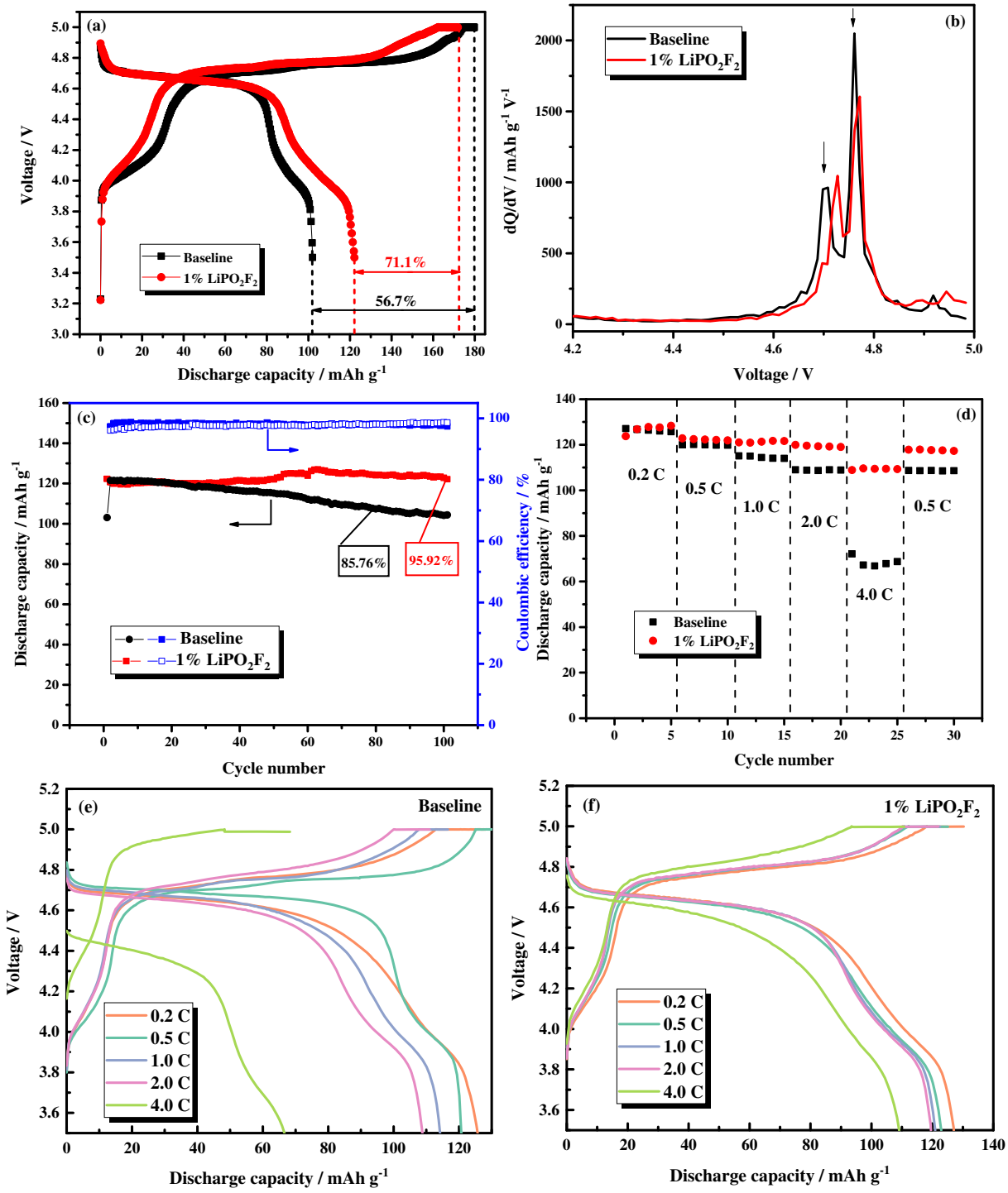

Fig. 4. Electrochemical performance of LNMO/Li with two electrolytes: (a) Charge-discharge curves recorded at initial cycle with 0.1 C rate; (b) corresponding dQ/dV profiles at initial charge process; (c) cycling performance; (d) rate performance; and charge-discharge curves at different rates with (e) baseline, (f) 1% $LiPO_2F_2$ electrolytes.

containing the additive is higher than that of the baseline electrolyte system. The improvement from the good cycle performance also indicates a good agreement of our prediction of the performance of the electrolyte system containing the additive. At the same time, we also further reviewed the changes in the rate performance of the two systems. Surprisingly, the system containing the additive not only has no attenuation but also improved. It delivers distinguished capacity retention rate even at high rate of 4.0 C and also reduces the irreversible capacity rate when the cells come back to 0.2 C. Further, we plotted the charge and discharge curves for different rates with two electrolytes in Fig. 4e and f. From the results, we can gain the information that with the increase of the rate, the discharge plateau in both systems goes down, and the polarization is more and more significant. However, in comparison, the system containing the additive shows no significant capacity decay, indicating that the additive effectively improved the electrode interface to improve the rate performance.

Further, we initially analyzed the film properties by impedance testing. In the impedance spectrum, we can analyze a large number of

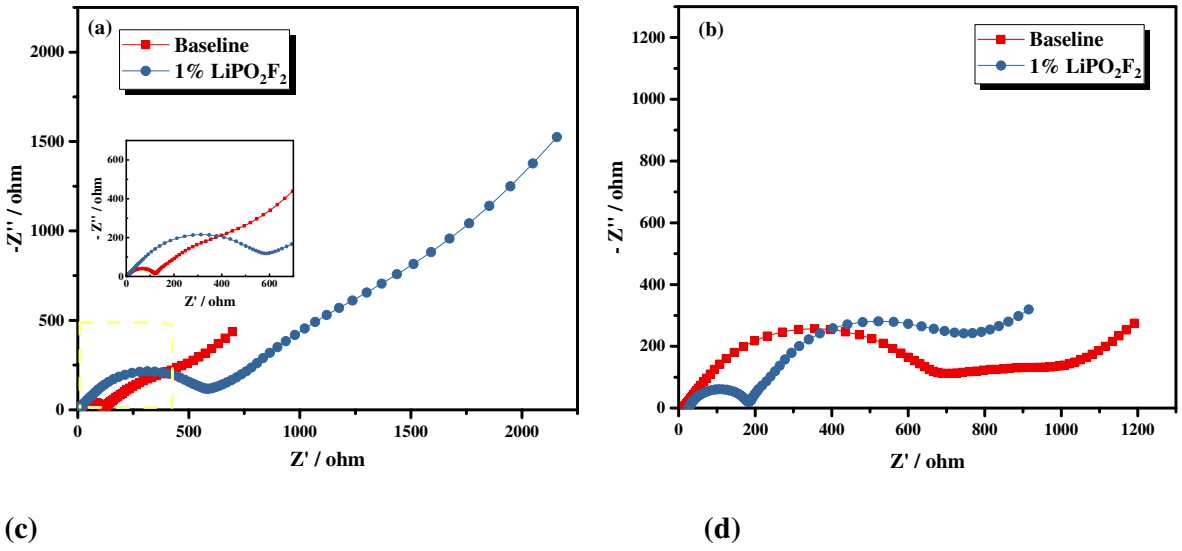

(c)

	Baseline		1% $LiPO_2F_2$	
	Activation stage /ohm	Cycling stage /ohm	Activation stage /ohm	Cycling stage /ohm
R_f	127.3	493.0	483.0	159.7
R_{ct}	196.1	346.0	384.1	404.6

(d)

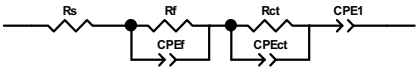

Fig. 5. EIS spectra of LNMO/Li cells with two electrolytes at different condition (at the fully delithiated state of 5.0 V): (a) activation stage; (b) after cycling stage; (c) impedance results of the simulation; and (d) corresponding equivalent circuit.

properties about the interface CEI film. Fig. 5 is an impedance test diagram and corresponding equivalent circuit diagram of the LNMO/Li half-cell of the two types of electrolytes in the fully charged state during the activation stage and after the completion of the cycling. In the impedance spectrum, the semicircle corresponding to the high frequency region represents the migration of lithium ions at the electrode/electrolyte interface. The semicircle of the intermediate frequency region corresponds to the well-known charge transfer process. The oblique line in the low frequency region corresponds to the diffusion of lithium ions from the outside into the interior of the electrode material or known as Warburg diffusion. After data simulated by the equivalent circuit, in the activation phase, it can be seen from the figure that the two electrolyte impedance patterns are consistent, but the R_f in the half-cell containing the additive electrolyte is significantly higher than the baseline electrolyte, indicating the film formed from the additive electrolyte was not perfect at first, and the baseline electrolyte was less decomposed at this time. In the cycle stage, from the data analysis, we found that the film resistance R_f of the baseline electrolyte increased significantly, but the film impedance of the additive electrolyte half-cell decreased to a certain extent, which can coincide with the cycle stability from the additive electrolyte.

3.3. Analysis of surface film properties

The results of the above analysis indicate the excellent effect of the $LiPO_2F_2$ additive in the electrolyte. The additive mainly produces a favorable substance, which oxidizes at the interface between the electrolyte and the electrode. The following chapters will qualitatively analyze the properties of the interface film by SEM, TEM, and XPS to reveal the mechanism by which the additive acts on the surface.

Fig. 6 is the SEM figures for the LNMO electrode with two electrolytes, which makes for the observation of surface morphology of the interface film (CEI film). Fig. 6a shows the surface of the LNMO electrode before cycling. It can be seen from the figure that the surface of the LNMO particles is smooth and the morphology of the polyhedron can be clearly seen. Fig. 6b and c are topographical views of the surface of the baseline electrolyte and the additive-added electrolyte after activation. From the figure can be seen that the LNMO surface of the two electrolytes is covered with a film. The film in Fig. 6c looks denser than in Fig. 6b, and the positive material LNMO particles can still be seen, which indicated that the film formed from additive electrolyte is not that thick. The film in Fig. 6b looks thick and loose, so that on the one hand the thicker film is not conducive to lithium ion transport, and the loose film still cannot hinder the further decomposition of the electrolyte, which will greatly reduce the capacity of the battery, accordingly, affects cycle stability. To gain more insight, the film covered on the particle was magnified for careful observation. Fig. 6d and e is partial enlarged views of the baseline electrolyte and the additive electrolyte, respectively. It can be observed that the film formed by the baseline electrolyte is thick and porous, and the original film becomes thinner and has an increase in density after the addition of the additive. This may be related to the decomposition product of the additive being different from the decomposition component of the lithium salt in the baseline electrolyte, which will be further analyzed later. Fig. 6f further magnifies the film formed by the additive, and it can be found that the surface film is a dense and uniform substance covering the electrode surface, so that the interface film with such a topography will help reduce the corrosion of the electrolyte to the electrode material, thereby improving the electrochemical performance. This also explains the excellent electrochemical performance of the additive electrolyte in the previous section.

The further film thickness was verified through TEM for two electrolytes shown in Fig. 7. From the figure we can observe that the state of the interface film derived from the two electrolytes is completely

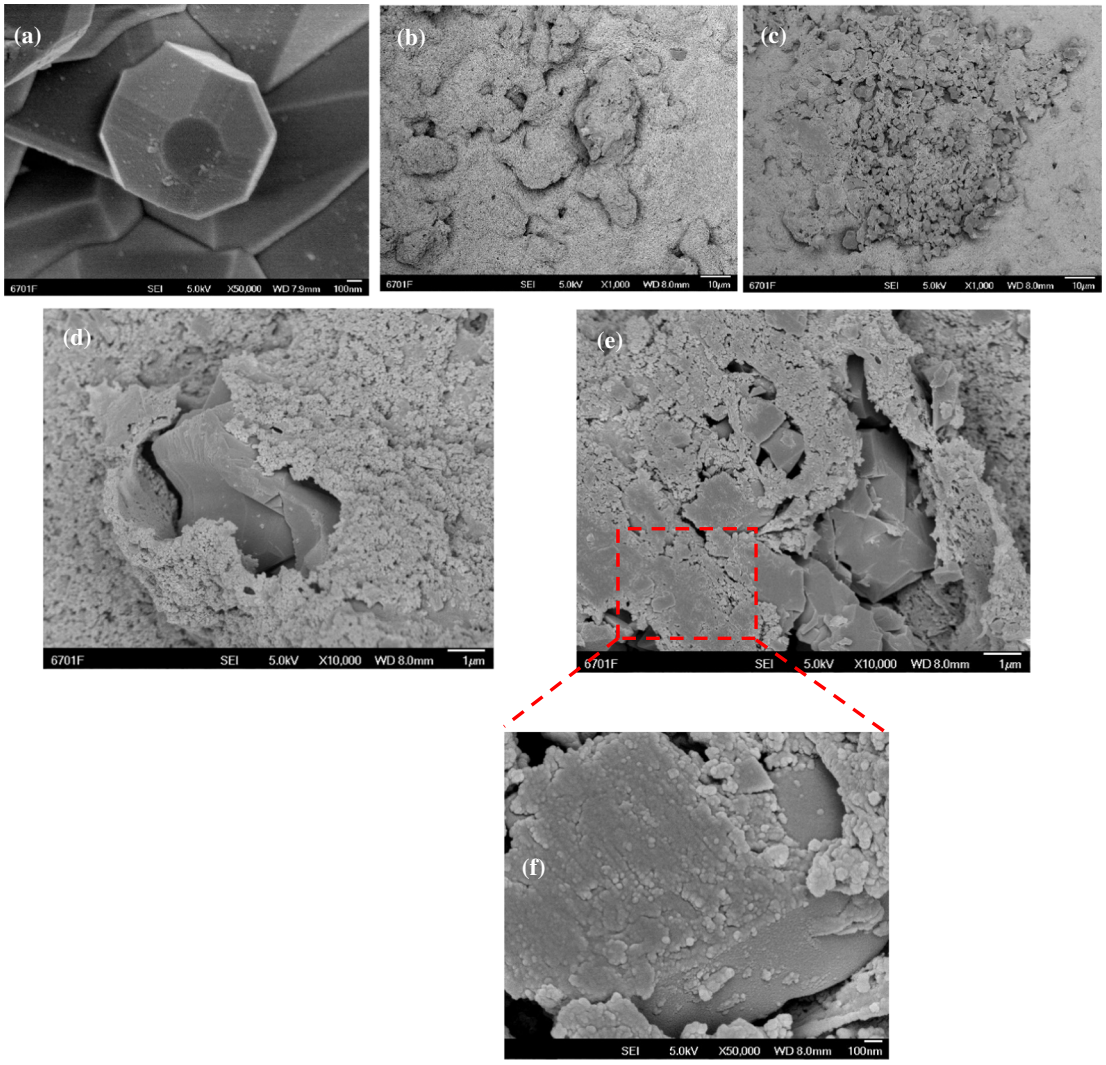

Fig. 6. SEM of the electrode surface for both of electrolytes at different condition (fully delithiated state of 5.0 V) (a) before cycling; (b) baseline electrolyte (×1000); (c) with additive electrolyte (×1000); (d) baseline electrolyte (×10,000); (e) with additive electrolyte (×10,000), and (f) additive electrolyte (×10,000).

different. It can be clearly observed from the figure that a very thick film formed by the baseline electrolyte shown in Fig. 7a covers the surface of the LNMO particles. Fig. 7b is an interface film of an electrolyte containing an additive. Although the film formed is not very uniform at the beginning but the film is thin, the portion of the electrode surface having a film can well protect the electrode surface. At the same time, we analyzed the elemental composition of the surface film of the additive, which is shown in Fig. 7c. From the analysis, we can see that the film contains a large amount of compounds containing P and F. And the closer to the outside of the material, the higher the distribution density of the two types of compounds, the approximate thickness of the film derived from the additive electrolyte can be estimated to be within about 50 nm by the distribution of elemental densities. The thickness of the film derived from the baseline electrolyte is much larger than 50 nm. From this result, we can visually confirm the conclusion of the impedance of Fig. 5.

Fig. 8 shows the XPS analysis of the interface film components derived from the two electrolytes. It can be clearly seen from the figure that there are some differences in the composition of the two CEI films, which is also caused by the difference in electrochemical properties of the two electrolytes, which is also the essential cause of the phenomenon. Peaks of 284.75 eV and 286.88 eV in C 1s can be detected on both electrolyte surfaces, which correspond to C—C and binder PVDF in the conductive material acetylene black in the electrode material. However, it can be found that the two types of peaks in the 1% $LiPO_2F_2$ electrolyte are significantly stronger than the baseline electrolyte, indicating that the film formed by the additive is relatively thin. The film component detected in the baseline electrolyte is mainly composed of inorganic substance Li_2CO_3, corresponding to the peak position of 289.48 eV in C 1s. The component of CEI film detected in the additive electrolyte is mainly composed of the organic substance $ROCO_2Li$, which corresponds to the peak position of 290.75 eV in C 1s. This also proves that the interfacial impedance of the 1% $LiPO_2F_2$ electrolyte becomes small because the lithium ion component of the organic compound in the CEI film is better in lithium ion conductivity than that of the inorganic lithium salt component. At the same time, we can observe that the interface film derived from the 1% $LiPO_2F_2$ electrolyte contains PO_4^{3-} component, corresponding to the 534.48 eV peak position of O 1s and the 134.13 eV peak position in P 2p, which also proves our previous verification of the decomposition mechanism of the additive $LiPO_2F_2$. In the O 1s spectrum, peak positions of approximately 529.68 eV and 544.08 eV can be detected in both electrolytes corresponding to oxide in the transition metal oxide and polymer $(-CH_2CH_2O-)_n$. In the F 1s spectrum, a strong LiF peak position can be detected in both electrolytes, and the corresponding peak position is about 686.58 eV. In the P 2p spectrum, we observed that the phosphorus-containing components in the baseline electrolyte are mainly Li_xPOF_y, Li_xPF_y, and POF_3. We have drawn the main components of the film derived from the two

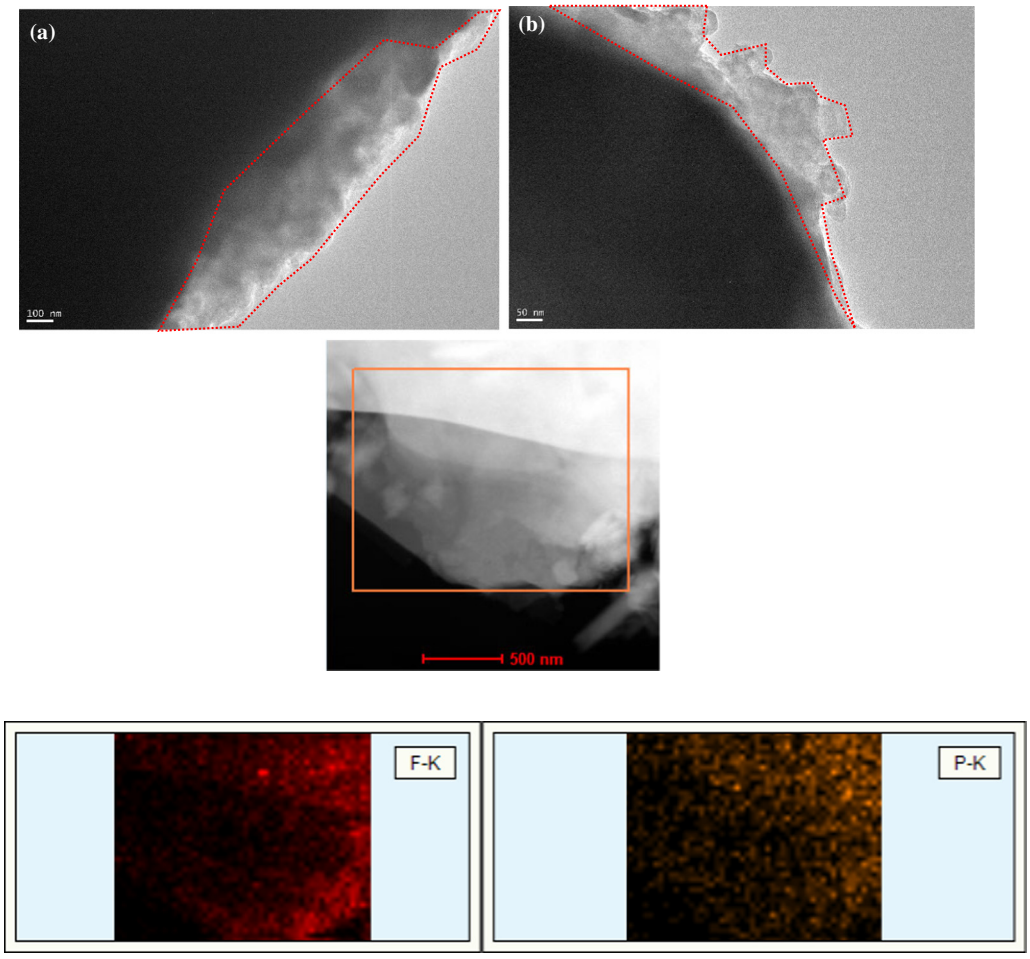

Fig. 7. TEM and mapping of LNMO/Li half cells for both of electrolytes at fully delithiated state of 5.0 V: (a) baseline electrolyte, (b) additive electrolyte, and (c) mapping for additive electrolyte.

electrolytes in the schematic diagram of Fig. 8e. From the figure, we can analyze that the CEI film derived from the additive electrolyte is mainly composed of organic carbonate and inorganic lithium phosphate. Such a component is beneficial to improve the transport performance of lithium ions, and a layer of Li_3PO_4 covers the electrode. The surface, according to the common ion effect, will decrease the subsequent decomposition of $LiPF_6$ and reduce the production of substances that are not conducive to lithium ion transport. This is also the reason for the improvement in battery performance after the addition of the additive, and its presence can reduce the generation of HF, which largely inhibits the dissolution of the transition metal ions. Thus, the cycle stability of the LNMO half-cell is greatly improved.

3.4. The analysis of effect mechanism for $LiPO_2F_2$

3.4.1. Quantum chemical calculation and analysis of film formation mechanism

Detailed mechanism of the action of additive can be further revealed by quantum chemical calculations. We further analyze the mechanism by optimizing the additive structure. As shown in Fig. S1, the additive $LiPO_2F_2$ is optimized by several structures, and finally the energy of the configuration of Fig. S3 is the lowest, so it is the most likely configuration in the electrolyte. Further analysis of this optimized structure reveals that Li^+ is equidistantly complexed with two oxygen atoms, resulting in a more stable structure in the electrolyte, which further explains the higher dissociation energy in Fig. 1b. Through the above analysis, we can infer the possible reaction routes of the two lithium salts as follows:

From the Table 1 can be analyzed that $LiPO_2F_2$ is easier to prioritize the generation of Li_3PO_4 than $LiPF_6$. The resulting Li_3PO_4 will inhibit the further decomposition of $LiPF_6$ (that is the reactions (6) (8) and (9)) to some extent. Meanwhile, the product of two lithium salts will react with the decomposition product from solvent shown in reactions (12) and (13). It can be probed that the product derived from $LiPF_6$ tends to produce deposition with increased impedance, in turn, $LiPO_2F_2$ is apt to produce more Li_3PO_4 to prevent the further decomposition of $LiPF_6$.

The decomposition of the above two salts is a chemical reaction. We found through analysis that the initial self-decomposition reaction of the two salts will be the final step of all subsequent possible reactions, that is, the reaction order of the reaction formulas (6) and (7) will determine the final reaction product. Therefore, we analyze the Gibbs free energy changes of the two reactions through quantum chemical calculations, and believe that the lower Gibbs free energy will occur preferentially. The specific calculation process is calculated by the Gaussian-4 (G4) thermodynamic combination method. The calculation process includes in the experimental section. As a result, as shown in Fig. S2, it is apparent that the Gibbs energy of the reaction (7) is much lower than that of the reaction (6), which indicates that the reaction (7) of the electrolyte on the surface of the positive electrode via the transition metal will occur preferentially. The subsequent reaction will proceed further. The preferential reaction of $LiPO_2F_2$ will promote the formation of Li_3PO_4 on the electrode surface, which will greatly hinder the decomposition of $LiPF_6$ under the same ion effect, thereby improving the electrochemical performance.

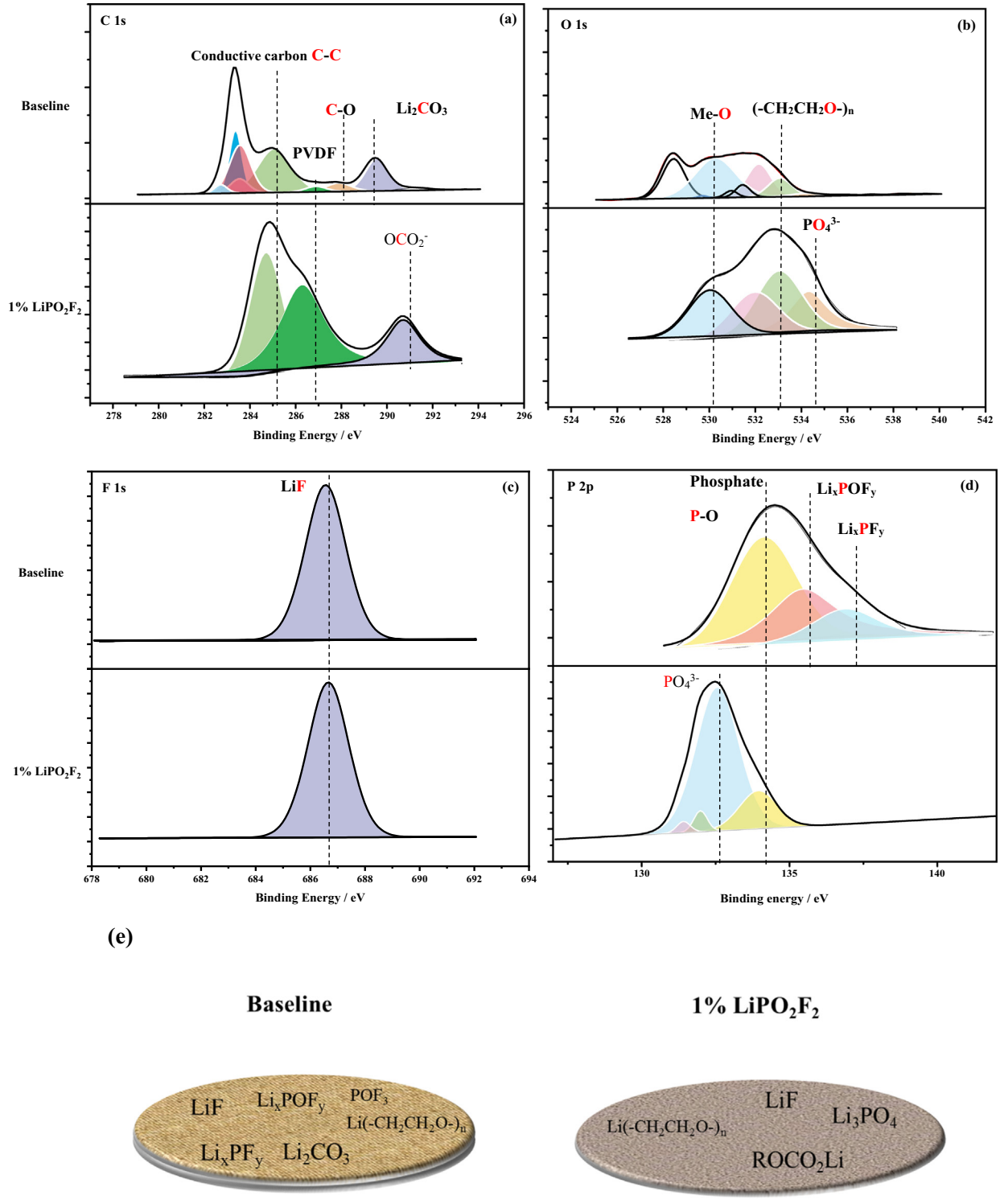

Fig. 8. XPS of LNMO/Li half cells for both of electrolytes after cycling at fully delithiated state of 5.0 V (a) C 1s, (b) O 1s, (c) F 1s, (d) P 2p, and (e) summary of surface film components for two electrolytes.

3.4.2. Some experiments for verification

In order to analyze the specific effect mechanism of the Li_3PO_4 on the surface of electrode, we have done a series of experiments to confirm this problem. We replaced the active material LNMO in the electrode with Li_2CO_3, LiF and Li_3PO_4 known as the inorganic substances that play a major role in CEI film to prepare the electrode sheets. And then above samples were used as cathode material in the cells with baseline electrolyte. After resting for 24 h, we tested AC impedance to certify the ability of these three inorganic substances to resist electrons. The results are shown in Fig. S3, it can be obviously shown from the figure and the analog value of R_{ct}, the Li_3PO_4 has the highest impedance value among the three inorganic substances. It shows that Li_3PO_4 has strong resistance to electrons causing the low current density, and the reaction resistance is relatively high, which can effectively reduce the reaction between electrolyte and active material. This inhibition can reduce the continuous growth of the interface film, which can cut down

Table 1
Mechanism reaction equation of $LiPF_6$ and $LiPO_2F_2$ in the non-aqueous electrolyte.

Self-decomposition reaction:
$LiPF_6 \rightarrow PF_5 + LiF$ (6)
$LiPO_2F_2 \rightarrow PO_2F + LiF$ (7)
Hydrolysis reaction:
$PF_5 + H_2O \rightarrow POF_3 + 2HF$ (8)
$POF_3 + H_2O \rightarrow PO_2F + 2HF$ (9)
$PO_2F + H_2O \rightarrow H_3PO_4 + HF$ (10)
$H_3PO_4 + 3Li^+ \rightarrow Li_3PO_4 + 3H^+$ (11)
Reaction with the decomposition product Li_2CO_3 from solvent:
$PF_5 + Li_2CO_3 \rightarrow LiPF_4O\downarrow + CO_2\uparrow + LiF$ (12)
$2PO_2F + 4Li_2CO_3 \rightarrow 2Li_3PO_4 + 4CO_2\uparrow + 2LiF$ (13)

the R_f as the result shown in Fig. 5b.

We sprayed the Li_3PO_4 solution on the LNMO electrode and then the electrode sheets were baked in a vacuum drying oven at 110 °C for 12 h to remove moisture and coat a small amount of Li_3PO_4 on the surface of electrode material. Whereafter, the samples coated with Li_3PO_4 were tested the electrochemical performance to verify the effect of Li_3PO_4 in the interface film. First of all, LSV was tested with the samples with and without spraying Li_3PO_4. As shown in Fig. S4, the oxidation potential for the samples sprayed Li_3PO_4 is significantly improved, which suggests that Li_3PO_4 can effectively reduce the decomposition of $LiPF_6$ electrolyte, which can be a good agreement with the statement in Fig. 4b. And then we test the cycle performance for the samples sprayed with Li_3PO_4 (Fig. S3), the capacity retention can be achieved 91.48% in 115 cycles. The relevant electrochemical performance test shows the good effect of the decomposition product. This will undoubtedly be a new idea for the coating of the positive electrode material or the artificial interface film.

In order to clarify the common ion effect of Li_3PO_4 in $LiPF_6$ based electrolyte, we added small amount of Li_3PO_4 powder after drying in an infrared oven in the baseline electrolyte. And then the electrolyte with and without adding Li_3PO_4 powder were put into the oven at 75 °C for a week. As shown in Fig. S5 that the color of two samples is completely different. The electrolyte without adding Li_3PO_4 turn red and the other only turn faint yellow, which can well prove that Li_3PO_4 powder can effectively inhibit the decomposition of $LiPF_6$ through the common ion effect.

4. Conclusions

After a series of evidences on the reaction mechanism of $LiPO_2F_2$, the key component Li_3PO_4 was probed out as the substance that plays a prime role in hindering the decomposition of $LiPF_6$. According to the spraying and replacing LNMO cathode material with Li_3PO_4, we conducted tests to demonstrate the mechanism by which Li_3PO_4 enhances interfacial stability under the common ion effect. Our work comprehensively reveals the mechanism of action of additives through direct (experimental verification and DFT calculation) and indirect means (surface testing). Thus, the relationship between cathode surface chemistry and CEI configuration has been established. As the result of the modification for the cathode surface derived from the product of electrolyte additive, the high energy and power density material LNMO with truncated octahedral structure can be greatly extended. This work advances a new insight into the interpretation of the effect of $LiPO_2F_2$ on the LNMO surface, which is critical for optimizing electrolyte components and fabricating high-energy-density Li-ion batteries with long service life. However, there are still some unresolved problems in our work, such as the insolubility of $LiPO_2F_2$ will limit its usage, the amount of 1% is its maximum dissolved amount in carbonate solvents. Whether the larger amount of $LiPO_2F_2$ has a greater impact on performance improvement is not known. Whether it is better synergy with solvents other than carbonates, such as sulfone solvents, is also worth exploring. Further research on the potential of $LiPO_2F_2$ deserves many researchers to probe into.

Acknowledgements

This work was supported by the Natural Science Foundation of China (no. 21766017), Science and Technology Project for Gansu Province (No. 18JR3RA160), and Lanzhou University of Technology Hongliu first-class discipline construction program.

Appendix A. Supplementary data

Supplementary data to this article can be found online at https://doi.org/10.1016/j.apsusc.2019.06.146.

References

[1] J. He, Y. Chen, P. Li, F. Fu, J. Liu, Z. Wang, Facile fabrication of RGO wrapped $LiMn_2O_4$ nanorods as a cathode with enhanced specific capacity, RCS Adv. 5 (2015) 80063–80068, https://doi.org/10.1039/C5RA09783E.
[2] J. He, G. Hartmann, M. Lee, G.S. Hwang, Y. Chen, A. Manthiram, Freestanding 1T MoS_2/graphene heterostructures as a highly efficient electrocatalyst for lithium polysulfides in Li–S batteries, 12 (2019) 344–350, https://doi.org/10.1039/C8EE03252A.
[3] X. Xu, S. Deng, H. Wang, J. Liu, H. Yan, Research progress in improving the cycling stability of high-voltage $LiNi_{0.5}Mn_{1.5}O_4$ cathode in lithium-ion battery, Nano-Micro Lett. 9 (2017) 22, https://doi.org/10.1007/s40820-016-0123-3.
[4] L. Xing, O. Borodin, Oxidation induced decomposition of ethylene carbonate from DFT calculations – importance of explicitly treating surrounding solvent, Phys. Chem. Chem. Phys. 14 (2012) 12838–12843, https://doi.org/10.1039/C2CP41103B.
[5] N.P.W. Pieczonka, Z. Liu, P. Lu, K.L. Olson, J. Moote, B.R. Powell, J.-H. Kim, Understanding transition-metal dissolution behavior in $LiNi_{0.5}Mn_{1.5}O_4$ high-voltage spinel for lithium ion batteries, J. Phys. Chem. C 117 (2013) 15947–15957, https://doi.org/10.1021/jp405158m.
[6] J. Mao, K. Dai, M. Xuan, G. Shao, R. Qiao, W. Yang, V.S. Battaglia, G. Liu, Effect of chromium and niobium doping on the morphology and electrochemical performance of high-voltage spinel $LiNi_{0.5}Mn_{1.5}O_4$ cathode material, ACS Appl. Mater. Interfaces 8 (2016) 9116–9124, https://doi.org/10.1021/acsami.6b00877.
[7] N.V. Kosova, I.A. Bobrikov, O.A. Podgornova, A.M. Balagurov, A.K. Gutakovskii, Peculiarities of structure, morphology, and electrochemistry of the doped 5-V spinel cathode materials $LiNi_{0.5-x}Mn_{1.5-y}M_{x+y}O_4$ (M = Co, Cr, Ti; x + y = 0.05) prepared by mechanochemical way, J. Solid State Electrochem. 20 (2016) 235–246, https://doi.org/10.1007/s10008-015-3015-4.
[8] Q. Xie, Z. Hu, C. Zhao, S. Zhang, K. Liu, LaF_3-coated $Li[Li_{0.2}Mn_{0.56}Ni_{0.16}Co_{0.08}]O_2$ as cathode material with improved electrochemical performance for lithium ion batteries, RSC Adv. 5 (2015) 50859–50864, https://doi.org/10.1039/C5RA06243H.
[9] J.S. Park, A.U. Mane, J.W. Elam, J.R. Croy, Amorphous metal fluoride passivation coatings prepared by atomic layer deposition on $LiCoO_2$ for Li-ion batteries, Chem. Mater. 27 (2015) 1917–1920, https://doi.org/10.1021/acs.chemmater.5b00603.
[10] X.-W. Gao, Y.-F. Deng, D. Wexler, G.-H. Chen, S.-L. Chou, H.-K. Liu, Z.-C. Shi, J.-Z. Wang, Improving the electrochemical performance of the $LiNi_{0.5}Mn_{1.5}O_4$ spinel by polypyrrole coating as a cathode material for the lithium-ion battery, J. Mater. Chem. A 3 (2015) 404–411, https://doi.org/10.1039/C4TA04018J.
[11] S. Li, D. Zhao, P. Wang, X. Cui, F. Tang, Electrochemical effect and mechanism of adiponitrile additive for high-voltage electrolyte, Electrochim. Acta 222 (2016) 668–677, https://doi.org/10.1016/j.electacta.2016.11.022.
[12] D. Zhao, P. Wang, X. Cui, L. Mao, C. Li, S. Li, Robust and sulfur-containing ingredient surface film to improve the electrochemical performance of LiDFOB-based high-voltage electrolyte, Electrochim. Acta 260 (2018) 536–548, https://doi.org/10.1016/j.electacta.2017.12.103.
[13] R. Hayes, G.G. Warr, R. Atkin, Structure and nanostructure in ionic liquids, Chem. Rev. 115 (2015) 6357–6426, https://doi.org/10.1021/cr500411q.
[14] J. Cha, J.-G. Han, J. Hwang, J. Cho, N.-S. Choi, Mechanisms for electrochemical performance enhancement by the salt-type electrolyte additive, lithium difluoro (oxalato)borate, in high-voltage lithium-ion batteries, J. Power Sources 357 (2017) 97–106, https://doi.org/10.1016/j.jpowsour.2017.04.094.
[15] L. Zhou, B.L. Lucht, Performance of lithium tetrafluorooxalatophosphate (LiFOP) electrolyte with propylene carbonate (PC), J. Power Sources 205 (2012) 439–448,

https://doi.org/10.1016/j.jpowsour.2012.01.067.
[16] Y. Dong, B.T. Young, Y. Zhang, T. Yoon, D.R. Heskett, Y. Hu, B.L. Lucht, Effect of lithium borate additives on cathode film formation in $LiNi_{0.5}Mn_{1.5}O_4$/Li cells, ACS Appl. Mater. Interfaces 9 (2017) 20467–20475, https://doi.org/10.1021/acsami.7b01481.
[17] M. Xu, L. Zhou, Y. Dong, Y. Chen, J. Demeaux, A.D. MacIntosh, A. Garsuch, B.L. Lucht, Development of novel lithium borate additives for designed surface modification of high voltage $LiNi_{0.5}Mn_{1.5}O_4$ cathodes, Energy Environ. Sci. 9 (2016) 1308–1319, https://doi.org/10.1039/C5EE03360H.
[18] I.A. Shkrob, Y. Zhu, T.W. Marin, D. Abraham, Reduction of carbonate electrolytes and the formation of solid-electrolyte interface (SEI) in Lithium-ion batteries. 1. Spectroscopic observations of radical intermediates generated in one-electron reduction of carbonates, J. Phys. Chem. C 117 (2013) 19255–19269, https://doi.org/10.1021/jp406274e.
[19] A.M. Andersson, D.P. Abraham, R. Haasch, S. MacLaren, J. Liu, K. Amine, Surface characterization of electrodes from high power lithium-ion batteries, J. Electrochem. Soc. 149 (2002) A1358–A1369, https://doi.org/10.1149/1.1505636.
[20] B. Zhang, M. Metzger, S. Solchenbach, M. Payne, S. Meini, H.A. Gasteiger, A. Garsuch, B.L. Lucht, Role of 1,3-propane sultone and vinylene carbonate in solid electrolyte interface formation and gas generation, J. Phys. Chem. C 119 (2015) 11337–11348, https://doi.org/10.1021/acs.jpcc.5b00072.
[21] B. Li, Y. Wang, W. Tu, Z. Wang, M. Xu, L. Xing, W. Li, Improving cyclic stability of lithium nickel manganese oxide cathode for high voltage lithium ion battery by modifying electrode/electrolyte interface with electrolyte additive, Electrochim. Acta 147 (2014) 636–642, https://doi.org/10.1016/j.electacta.2014.09.151.
[22] K.-E. Kim, J.Y. Jang, I. Park, M.-H. Woo, M.-H. Jeong, W.C. Shin, M. Ue, N.-S. Choi, A combination of lithium difluorophosphate and vinylene carbonate as reducible additives to improve cycling performance of graphite electrodes at high rates, Electrochem. Commun. 61 (2015) 121–124, https://doi.org/10.1016/j.elecom.2015.10.013.
[23] G. Yang, J. Shi, C. Shen, S. Wang, L. Xia, H. Hu, H. Luo, Y. Xia, Z. Liu, Improving the cyclability performance of lithium-ion batteries by introducing lithium difluorophosphate ($LiPO_2F_2$) additive, RSC Adv. 7 (2017) 26052–26059, https://doi.org/10.1039/C7RA03926C.
[24] B. Yang, H. Zhang, L. Yu, W. Fan, D. Huang, Lithium difluorophosphate as an additive to improve the low temperature performance of $LiNi_{0.5}Co_{0.2}Mn_{0.3}O_2$/graphite cells, Electrochim. Acta 221 (2016) 107–114, https://doi.org/10.1016/j.electacta.2016.10.037.
[25] W. Zhao, G. Zheng, M. Lin, W. Zhao, D. Li, X. Guan, Y. Ji, G.F. Ortiz, Y. Yang, Toward a stable solid-electrolyte-interfaces on nickel-rich cathodes: $LiPO_2F_2$ salt-type additive and its working mechanism for $LiNi_{0.5}Mn_{0.25}Co_{0.25}O_2$ cathodes, J. Power Sources 380 (2018) 149–157, https://doi.org/10.1016/j.jpowsour.2018.01.041.
[26] Q.Q. Liu, L. Ma, C.Y. Du, J.R. Dahn, Effects of the $LiPO_2F_2$ additive on unwanted lithium plating in lithium-ion cells, Electrochim. Acta 263 (2018) 237–248, https://doi.org/10.1016/j.electacta.2018.01.058.
[27] M.J. Frisch, G.W. Trucks, H.B. Schlegel, et al., Gaussian 09, Revision D.01, Gaussian, Inc., Wallingford CT, 2016.
[28] H. Xiao, H. Wu, X. Chi, SCE: grid environment for scientific computing, in: P. Vicat-Blanc Primet, T. Kudoh, J. Mambretti (Eds.), Networks for Grid Applications. GridNets 2008. Lecture Notes of the Institute for Computer Sciences, Social Informatics and Telecommunications Engineering, vol 2, Springer, Berlin, Heidelberg, 2009.
[29] Tian Lu, Feiwu Chen, Multiwfn: a multifunctional wavefunction analyzer, J. Comput. Chem. 33 (2012) 580–592.
[30] A.V. Marenich, J. Ho, M.L. Coote, et al., Computational electrochemistry: prediction of liquid-phase reduction potentials, Phys. Chem. Chem. Phys. 16 (2014) 15068–15106, https://doi.org/10.1039/C4CP01572J.
[31] L.A. Curtiss, P.C. Redfern, K. Raghavachari, Gaussian-4 theory, J. Chem. Phys. 126 (2007) 124107, , https://doi.org/10.1063/1.2436888.
[32] C.-H. Jo, D.-H. Cho, H.-J. Noh, H. Yashiro, Y.-K. Sun, S.T. Myung, An effective method to reduce residual lithium compounds on Ni-rich $Li[Ni_{0.6}Co_{0.2}Mn_{0.2}]O_2$ active material using a phosphoric acid derived Li_3PO_4 nanolayer, Nano Res. 8 (2015) 1464–1479, https://doi.org/10.1007/s12274-014-0631-8.